Department of Precision and Microsystems Engineering

Towards improved orthopaedic drilling at hard to reach bone sites; The design of a compact Self-Feeding Angled Drill Attachment (SFADA)

Jorik van der Laan

Report No : 2020.014
Coach : J.W. Spronck
Professor : J.W. Spronck
Specialisation : Mechatronic System Design
Type of report : MSc Thesis
Date : May 2020

TU Delft Delft University of Technology

Challenge the future

Towards improved bone drilling at hard to reach bone sites; the design of a compact Self-Feeding Angled Drill Attachment (SFADA)

by

Jorik van der Laan

to obtain the degree of Master of Science

at the Delft University of Technology,

to be defended publicly on Wednesday May 27, 2020 at 12:45 PM.

Student number:	4298926	
Thesis committee:	Ir. J. W. Spronck,	TU Delft, supervisor
	Dr. J. J. van den Dobbelsteen,	TU Delft
	Ir. J. Nijssen,	TU Delft

This thesis is confidential and cannot be made public until May 27, 2021.

Preface

The thesis presented in this report is the final part of the master studies mechanical engineering. The aim of the thesis is to improve the bone drilling process at hard to reach bone sites. The final design can be of great use to orthopaedic surgeons but requires further development towards a medical product.

This thesis is the continuation of a project initiated by Laurens Krijgsman, Jo Spronck and Kees Bartlema. Their research was aimed at deriving a set of functional requirements that reduce thermonecrosis in pelvic bone drilling. New insights were found about the contribution of radial forces and moments on thermonecrosis. A novel device was developed to perform drilling in a controlled manner such that this does not occur. My thesis project is an extension of this design, with a focus on other complications in bone drilling and a more user friendly device. The project has greatly sparked my interest, especially the interaction between mechanical design and the medical environment. The project contained almost every aspect of the mechanical design process. From establishing requirements with surgeons, to fabrication in the workshop and verification in the lab. The project will be continued by Joost Schots, who will focus on the bone drilling procedure as a whole, with a focus on the positioning and fixation of the device. I wish him all the best with his project.

With the completion of this thesis, the end my studies is almost reached. I'm grateful for the opportunity to finish my studies and would like to thank everyone that made it possible in some shape or form.

Jorik van der Laan
Delft, May 2020

Contents

Abstract

Bone drilling is a crucial part of orthopaedic surgery. Internal fixation is a common orthopaedic procedure that requires drilling to improve healing of bone fractures. Tight spaces around hard to reach bone fractures impede the surgeon during the procedure. As a result there is an increased risk of complications such as thermonecrosis, overshoot into soft tissue, micro-crack formation and drill bit breakage. Therefore, a novel procedure is proposed, where drilling is done using a compact Self-Feeding Angled Drill Attachment (SFADA). The SFADA is a crucial part of the new procedure, because it can generate a controlled feed in a confined space. Four concepts were developed that met these functionalities. Based on the design specifications a final concept was selected. The concept based on a differential thread and a lead/lag bevel gear was deemed the most feasible. Materials and dimensions were assigned to the mechanism based on an analysis of the critical components. A compact demonstrator of 80x40x36 mm was built. Measurements were performed and the results showed the SFADA's ability to perform controlled drilling in a confined space. Furthermore, the SFADA can generate a speed of 1500 rpm and feed of 1.5 mm/s, with load forces and torques up to respectively 20 N and 0.2 Nm. The design of the SFADA is an important step in the improvement of bone drilling at hard to reach bone sites.

1 Introduction

Bone drilling is required in multiple orthopaedic procedures. One of these procedures is internal fixation, where a plate is fixed over a fracture to improve bone healing quality [1]. To attach the plate over the fracture holes are drilled. Screws are fit into the holes and connect the bone to the plate [2]. During this procedure an accessible fracture site is desired with a large operational volume available over the bone site. This allows the surgeon to position itself and the drill over the fracture for optimal control of the drilling device. This is not possible in some procedures because the patients body obstruct the surgeon. For example fractures in the clavicle or pelvic ring are hard to reach and the surgeon has to operate in a tight space. This limits the control over the device and make the procedure more prone to mistakes. As a result the risk of complications increases. Common complications in bone drilling are thermonecrosis, drill bit breakage, hole wall micro-fractions and overshoot into soft tissue [3–5]

Heating of the bone due to excessive friction can cause necrosis of bone cells [6]. This is known as thermonecrosis and permanently damages the bone. Radial movement of the drill causes stresses in the drill hole walls and the drill bit. This can result in both micro-crack formation in the walls [7, 8] as breaking of the drill bit [3, 9]. When the drilling depth overshoots the length of the bone, underlying tissue such as blood vessels, tendons and muscle can be damaged [10].

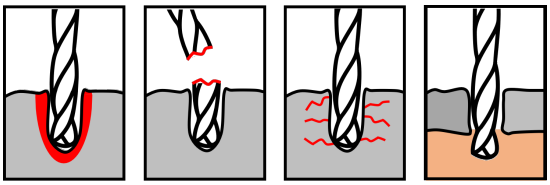

Figure 1: Four common bone drilling complications: Thermonecrosis, drill bit breakage, hole wall micro-fractions and overshoot into soft tissue

During the conventional drilling procedure, the surgeon aims to minimize complications. This is done by maintaining a steady position of the drill, while the surgeon slowly feeds the drill bit into the bone. When the drill bit approaches the end of the bone, the surgeon experiences a decrease in resistance and a change in sound. This indicates that drilling quickly has to be ceased to prevent overshoot. The procedure is complicated, and previous research has presented devices that assist the surgeon during

drilling [11] by reducing the complexity. An overview of devices and methods relevant to drilling at hard to reach bone sites will be presented in the following subsection.

1.1 Prior Studies

Early developments in assisted drilling devices presented the design by Alotta [12]. The device made use of a slowly retracting bone stand, which suited two purposes. The retracting motion slowly fed the drill bit into the bone, which made for controlled drilling. Additionally, the stand fixed the position of the drill bit, preventing any unwanted movement. The system measured the thrust force and could control the drill depth based on large differences in thrust signal. The device by Alotta is the first instance of assisted bone drilling found in literature and displays three key functionalities: a controlled feed, position fixation and hole depth control. Further developments since Alotta presented different approaches to achieve these functionalities, all with there own benefits. For each functionality, relevant methods will be discussed.

The ability to control the feed of the drill bit is an important trait in assisted drilling devices. It allows for control of the feed variable, and enables drilling under conditions at which complications do not occur [13]. Many instances found in literature used an extra actuator to generate this feed [12, 14, 15], which made the device bulky. To reduce the size of the device that had to be manoeuvred over the drilling site, actuation could be place externally. Gregoor [16] applied this concept by the use of a hydro powered drill. Pressurised water was fed to the device and converted to rotation of the drill. Krijgsman [17] also used this principle by drilling with a satellite drill attachment. The satellite consisted of a drill bit connected to a linear carriage. Rotation was transferred to the drill bit by means of a flexible drive cable, and translation was generated by a Bowden cable mechanism. An alternative approach to reduce device size is a self-feeding mechanism. Self-feeding is the ability of the mechanism to generate both rotation and translation of the drill bit from a single input. Only one actuator is required to generate both rotation and feed. Shim et al. [18] drove an angled friction wheel, to generate the self-feeding motion. Walsh et al. [19] designed a CT-compatible medical drilling stylet, which generated a coupled feed and rotation using a differential lead screw mechanism. Both systems require the fixation of the device to an external frame to counter thrust forces.

Figure 2: Drilling performed using the ODRO [20] reduces complications, but introduces a very bulky device.

Depth control ensures that the drill bit does not overshoot the bone [10]. Whenever the end of the bone is reached, drilling torque decreases due to the reduced resistance encountered by the drill bit. The majority of the depth control systems in literature apply this method [12, 21–23]. Direct measurement of the thrust signal was used by Brett et al. [22] Drilling was stopped if the feed force decreases and the drill torque increases for six consecu-

tive samples. Bouazza-Marouf et al. [23] applied a simpler form of the modified Kalman Filter to a 'force difference for successive samples (FDSS)' signal. Alternative sensing methods were found in literature. The DRIBON [21] relied uniquely on a linear encoder for displacement measurements of the drill. A constant feed was applied until the remaining bone layer was very thin. When breakthrough was about to happen, the stiffness of the layer decreased and feed speed increased rapidly, indicating the end of the bone. Torun et al. [24] developed a system capable of real time analysis of sounds recorded during the drilling procedure. Sounds differed depending on resistance, so a change in sound could indicate the end of the bone. Measurements of the sound during the process did not have to be within the drilling device itself, allowing for external sensing.

Another important aspect to reduce complications is positioning of the drill [17]. A fixed drill position prevents radial movements of the drill bit. This reduces the risk of drill bit breakage, micro-cracks and thermonecrosis [17]. Devices were found that do not require physical connection to the patient or the surgeon but were fixed to an outside frame [18, 25]. Hessinger et al. [26] used IR-LED's to track drill orientation and location, and fed this information back to the user. An alternative design by Hessinger et al. [27] controlled position with a seven degree of freedom exoskeleton attached to the surgeon. The device by Krijgsman [17] introduced the concept of constraining movement of the device by the attachment of retractable stands to the area surrounding the fracture.

The devices aforementioned showed good approaches at countering complications that can occur during bone drilling. Three functionalities are important to reduce bone drilling complications: generate a controlled thrust, maintain a steady position and control drill hole depth. Devices were found that combine these functionalities, but are too bulky to fit the tight spaces at hard to reach bone sites. An example can be seen in figure 2. Prior research showed that device size can be reduced by external placement of the actuator [16], and coupling of rotation and translation of the drill bit using a self-feeding mechanism [18, 19]. Additionally, the self-feeding property prevents overshoot. The drill cannot overshoot the bone, since feed is coupled to rotation of the drill bit. This would also remove the need for a depth control mechanism. A drilling device that combines self-feeding with external placement of the actuator would fit the tight spaces at hard to reach bone sites. No instance of such a device was found in literature and therefore drilling at complex bone sites will remain prone to complications.

1.2 Contribution

To improve drilling at hard to reach bone sites, a novel procedure is introduced. Drilling is performed using a compact Self-Feeding Angled Drill Attachment. The attachment is positioned and fixed at the bone site. A cordless drill can be held externally and angled with respect to drilling direction. Driving the SFADA generates self-feeding drilling, where the drill bit is automatically rotated and fed into the bone at the same time. When the surgeon feels and hears that the end of the bone is reached, they cease drilling. The SFADA reduces operational volume, to enable drilling in a tight space.

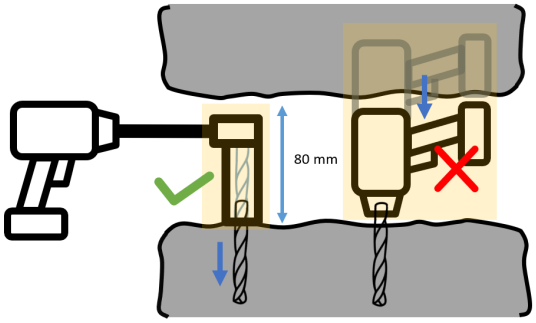

Figure 3: Drilling with the SFADA reduces operational volume

Additionally, the procedure with a SFADA reduces complications because of three reasons. Firstly, the feed can be applied under condi-

tions at which necrosis does not occur. Secondly, the fixed position of the device prevents radial movements of the drill bit, preventing thermonecrosis and drill bit breakage. And lastly, the feed is coupled to the rotation and independent of bone resistance, so overshoot is not possible.

This report will describe the design of the compact Self-Feeding Angled Drill Attachment (SFADA), a key component to the new procedure. The goal is to generate a controlled feed in a confined volume, using a self-feeding mechanism and external placement of the actuator. The new procedure also requires the SFADA to be fixed to the bone. A different research will focus on this part, and for the remainder of the report the SFADA is considered to be fixed to the bone.

2 Design Specifications

Based on previous research and meetings with trauma surgeons prof. M. van der Elst M.D. and K.A. Bartlema M.D. a set of specifications were derived that the design should satisfy. The set of specifications were taken into consideration throughout the project. Two different types of specifications can be distinguished, namely the functional requirements and user needs. The functional requirement are measurable physical values of the design. In order to improve the bone drilling process, the design should meet all requirements. The requirements are verified via diverse measurements that are described in section 5 of this report. The second consideration are the user needs. The user needs are also important to take into consideration but these are not as strict and measurable as the functional requirements. The details and origins of all specifications will be discussed in this section.

2.1 Functional Requirements

To improve orthopaedic bone drilling, the SFADA must reduce the risk of complications. One of the complications is thermonecrosis, which is caused by excessive frictional heating in the drill hole. Previous research by Krijgsman presented a set of drilling variables at which thermonecrosis does not occur [17]. A 4 mm drill bit is commonly used in orthopaedic bone drilling. Therefore, this bit was used in this study. For this bit, drilling should be performed at a rotational speed of 1500 rpm and feed rate of 1.5 mm/s. Maximum reaction force and torque at these speeds are 0.2 Nm and 20 N respectively.

Table 1: SFADA functional requirements

Functional Requirement	Value	Unit
Dimensions	80x40x40	mm
Drill Torque	0.2	Nm
Thrust Force	20	N
Rotational Speed	1500	rpm
Feed Speed	1.5	mm/s

The limited space available over the bone site differs for every procedure. Conversations with surgeons gave maximum device dimensions of 80x40x40 mm to fit most procedures. The dimensions are based on the surgeons' experiences. An overview of all functional requirements with corresponding values can be found in the table 1.

2.2 User Needs

Since the drilling mechanism is used in a medical environment, a sterile instrument is required to prevent contamination of the operation site. This can be done by sterilizing the system after use to eliminate all microorganisms. The device should have no small cracks or tight spaces in which contamination could remain present. Another solution is to make the system fully disposable. So that after use, the device can be discarded.

To ensure the safety of the patient and surgeon, direct control of the drill is necessary. The system can only remain active as long as a button is pushed. Removal of this signal should result in immediate standstill of the device. This allows for easy intervention if failure occurs.

During drilling, it is possible that the drill bit gets stuck due to unforeseen obstructions. Therefore, it must be easy to detach the drill bit from the device. After detachment from the device the drill bit can be safely removed from the bone site.

The SFADA will be in close proximity to the patient. As a result the device will be exposed to bodily fluids and saline solution. The presence of moisture can cause short circuits to open circuits, change friction values or wash out lubricants. These factors should be taken into account during the design.

Besides feeding into the bone, retracting from the bone is an equally important aspect of the drilling procedure. Without this retraction it will not be possible to remove the device from the drilling site. Reversing the actuator should retract the drill bit from the hole.

During the process of internal fixation X-ray images are taken of the drill bit and fracture to verify drill bit location and orientation. Metal components cast a shadow over the images, obstructing the surgeons view of the bone site. Where possible, the choice for non-metal materials should be considered to reduce X-ray image shadows.

The SFADA should fully retract the drill bit into the device, which contributes to a compact design. From this initial size, stroke should be as large as possible. This enables drilling in a range of bone sizes.

When the drill bit reaches the end of the bone, the surgeon stops drilling. The end of the bone is indicated by a change in sounds exerted by the drill. The novel procedure must not interfere with this property. The new drilling procedure should remain familiar to the surgeon, such that his experience on bone drilling sounds is useful.

3 Conceptual Design

Key functionalities of the SFADA are its ability to generate self-feeding and an angled conversion of rotation, all contained in a compact design. This enables a reduced operational volume and a controlled feed. During the project, several concepts were developed that meet these functionalities. The focus is on the self-feeding in particular, of which only limited accounts were found in literature [18,19]. Based on a number of criteria a favourable concept is selected. Additional challenges will be discussed and two separate solutions will be presented. A proof of concept study will declare the eventual final concept.

3.1 Self-Feeding Concept

Self-feeding is the ability of the mechanism to generate both rotation and translation of the drill bit from a single input. It reduces operational volume, because the attachment can be fixed in a single place when drilling, in contrary to conventional drilling methods where the entire device is moved to generate feed. Additionally, it enables a controlled application of feed and prevents overshoot. To achieve self-feeding, several mechanisms were developed; a description of the generated concepts:

Concept A uses angled rolling friction [18]. A drill shaft is constrained, but free to rotate and translate about its longitudinal axis. A wheel is placed on the shaft, such that the wheel's surface touches the shaft. The angled rolling friction applies both an axial and tangential force to the shaft, generating rotation and translation at the same time. Input rotation is redirected to the angled wheel via a constant-velocity joint.

Concept B is based on a hydraulic driven motor and piston [16]. Pressurised water is fed into the device through a flexible tube, which is converted into rotation using an external gear motor. The outgoing shaft is fixed to a piston to which the drill bit is connected. Redirection of the pressurised water into the rotating piston causes self-feeding. Positioning of the actuator is variable due to the flexible input tube.

Concept C adapts a previous design based on a sliding feed carriage [17]. A flexible drive shaft transfers rotation to a drill bit on a

sliding feed carriage. The carriage is free to translate within the designs frame. The rotation of the drill bit causes winding of a wire onto a coil. The wire is fixed to both the frame and the carriage, such that the winding causes feed while rotating the drill bit.

Concept D makes use of the screw motion generated in a thread [19]. The drill bit is fixed to an outside threaded part which is mostly constrained, but free to rotate and translate about the drilling direction. This component is screwed into a fixed inner threaded part. The screwing motion makes for the self-feeding functionality. A right angle transmission is achieved using bevel gears.

The user needs from the previous section were translated to the criteria in the following chart. Each concept will be scored from 0 to 2, and the concept with the highest score is considered to be the most feasible for further development of a SFADA. The criteria, scores and concepts can be seen in the decision-matrix table 2. An extended description of the concepts, criteria and scoring can be found in appendix A. Based on arguments displayed in this chart, the thread and gear concept is the most feasible solution for the design of a SFADA. The concept scores well over almost all criteria, besides the risk of jamming. Close attention has to be paid to prevent this from occuring.

3.2 Thread Concept

The selected concept uses the screw-motion that is generated via the connection of the two threaded parts. The right angle transmission is achieved by a bevel gear set. A property of thread is a constant relation between input speed, output speed and feed speed dependent on thread lead. The relation is shown in the equation 1 below:

$$\omega_{drill} = \frac{2\pi\nu}{L} \tag{1}$$

Where ν is the feed rate and L the thread lead.

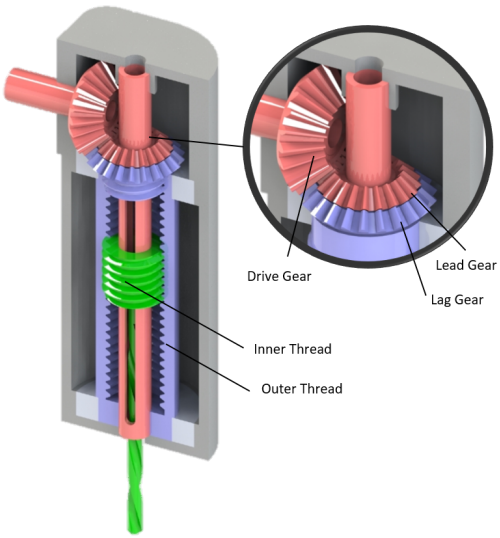

Figure 4: Section view of concept C1 with a close up of the lead/lag gear set

For the given functional requirements there can be found that a feed of 1.5 mm/s will result in a required lead of 60 μm. A thread this small can not be fabricated, let alone handle the loads. Thread lead should be larger, while still satisfying the required speeds. Two concepts that will be presented in the following sections both provide a different solution to the problem. The first concept uses a differential thread mechanism. The second concept uses a cycloidal gear thread mechanism.

3.2.1 Concept C1: Differential Thread Mechanism

A lead screw mechanism is commonly used to convert a rotation into a translation. In a conventional lead screw a nut is screwed onto a thread. It is free to translate, but constrained in rotation. By turning the thread the nut translates along the thread. If the nut was free to rotate, but driven at a different speed than the thread, it would still translate, but at a reduced speed. The following concept is based on this principle.

The red drive gear will drive both the lead gear

Table 2: Decision-matrix for concept selection

Concept	**A** Angled Friction Wheel	**B** Flexible drive, carriage and cable	**C** Thread and gears	**D** Hydro motor and cylinder
Required Loads	0	1	2	1
No Slip	0	2	2	2
No Jamming	2	1	0	1
Reverse	2	0	2	0
Sensing Interference	2	1	2	0
Manufacturability	1	2	2	0
Total	7	7	**11**	4

and the lag gear at the same time. The lead gear turns the inner thread and the lag gear the outer thread. The addition of a tooth to the lag gear creates a speed difference between the threaded components. This reduces the feed speed. The feed is a result of the difference between the two speeds, and the lead of the thread, as can be seen in the equation below. ω_{lead} is the speed of the inner gear, ω_{lag} the speed of the outer.

$$\nu = \frac{(\omega_{lead} - \omega_{lag})}{2\pi} L \tag{2}$$

The proposed concept drives two gears with the same average diameter, but different teeth numbers, which results in different modules. This would lead to smaller spaces between teeth in the lagging gear causing wear and jamming. To account for this, space between the teeth is increased by reducing tooth width on the lag gear [28].

The reduction in the gear assembly is based on the number of teeth on each gear. Combining this with equation 1 gives the following design rule. It shows that the ratio between number of teeth on the lag gear N_{lag} and lead gear N_{lead} is dependent on feed, speed and thread lead. In order for this concept to achieve the required performance, the following design rule should be satisfied.

$$\frac{N_{lag}}{N_{lag} - N_{lead}} = \frac{\omega_{drill}}{2\pi\nu} L \tag{3}$$

3.2.2 Concept C2: Cycloid Thread Mechanism

Cycloidal drives are transmission systems capable of achieving large speed reductions within a compact design [29]. With space being limited in the SFADA, the cycloid drive can be used to reduce the drill speed within a small footprint.

The red input shaft is driven at desired drilling speed. Using a bevel gear set, the rotation gets redirected to the red slotted tube. A pin fits in this slot, and connects to both the drill bit on the inside and the eccentric cam on the outside. This combination is free to translate along the slotted tube, but fixed to rotate with the tube. The eccentric's cam rotation results in rotation of the cycloid cam. The cycloid 'walks' along the outside wall, rotating the pins about the wall's lobes. The reduced rotation of the blue cam is transferred to the green drive screw using hole pins. Thread is cut through the pin profile on the outside, in which the drive screw is slowly screwed. Cycloid drive reduction is determined by the number of lobes N_{lobes} on the cam, and the number of pins N_{pins} on the outside ring. The *design rule* for concept C2 is set by combining gear ratios with equation 1.

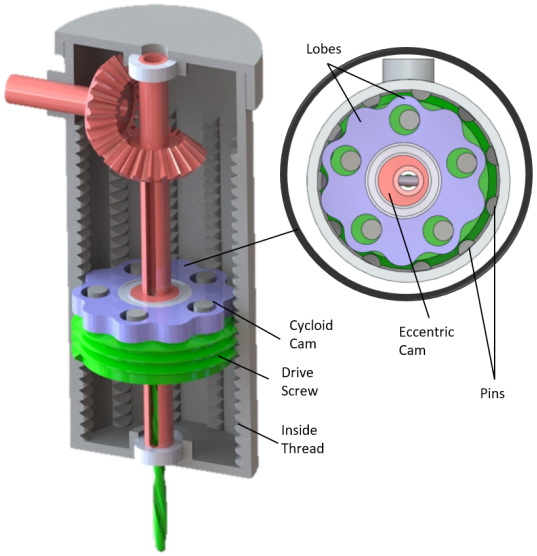

Figure 5: Section view of concept C2 with an overhead view of the cycloid gear

A fixed ratio between pins and lobes is required for the given feed, speed and lead.

$$\frac{N_{pins} - N_{lobes}}{N_{lobes}} = \frac{\omega_{drill}}{2\pi\nu} L \tag{4}$$

3.3 Final Concept Selection

Both presented designs show promising performance. The differential thread, as well as the cycloid gear should be capable of achieving desired speeds if the design rules are satisfied. Reconsidering the criteria in table 2 shows not much difference in scoring, since the designs are derived from the same thread principle.

To get a hands on feeling of the performance, concept proof models were made for both designs. This introduced the problem caused by the eccentric movement of the cycloid cam in concept C2. Due to this movement, the SFADA will exert radial vibrations on the drill bit and bone fixture. Prior research by Krijgsman [30] has already shown that radial forces on the drill bit will increase thermonecrosis, thus counteracting the goal of the SFADA. Stacking additional cycloid cams could decrease vibrations, but increases transmission dimensions. Concept C1, which uses the differential thread mechanism, was seen the most feasible solution for a SFADA.

4 Detailed SFADA Design

The following section discusses how the design was developed and what considerations were made to reach the final form. An overview of the design with all components and their functionalities will be given. Critical components in the design will be analysed separately and combined in the concluding section where total system performance is discussed.

4.1 Design Overview

In figure 6 below, the CAD model of the final SFADA design can be found. It displays the names of important components. The colours indicate components which move in unison. A rundown of the mechanism; The yellow drive shaft is driven by a cordless power drill. Rotation of drive gear cause both the lead gear and lag gear to rotate. The lead gear is fixed to the slotted tube, and the lag gear to the threaded tube. Connecting the drill bit to the drive screw with the slot pin (not shown in figure 6) allows for transfer of torque while free to translate. Rotation of the drive gear generates a coupled rotation and translation of the drill bit.

The maximum dimensions of the design are 80x40x36 mm, conform the functional requirements. The stroke of the drill bit is defined by the threaded tube length and drive screw height, which gives a stroke of 40mm. The drill bit is connected to the slot pin using a bayonet lock, making it easily detachable. The small spaces in the thread and gear can contain moisture after use. The device should be disposed after use to prevent contamination.

4.2 Critical Component Analysis

In order to perform bone drilling, the device should withstand the forces and torques en-

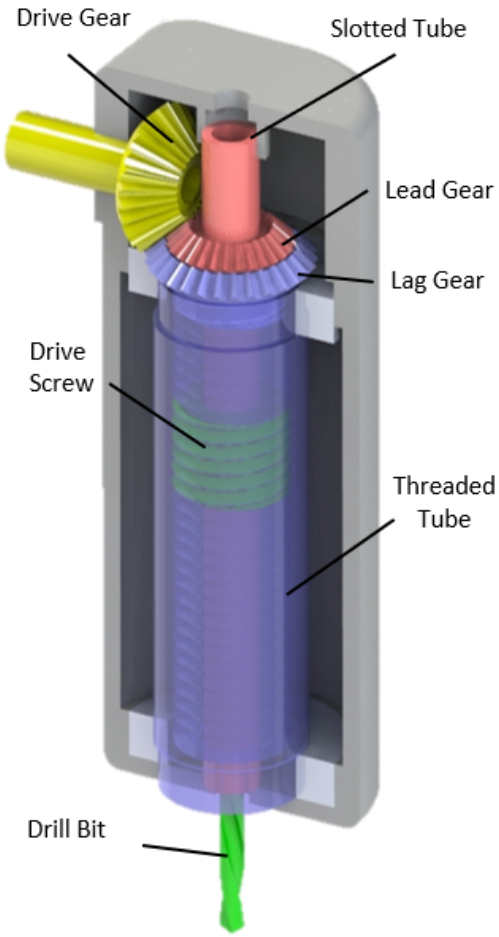

Figure 6: Section view of the final design with critical components highlighted

countered without failing. Insufficient strength of the components can cause stresses to exceed material yield limits. This would result in plastic deformation of critical components, which compromises device functioning. To ensure no plastic deformation, equivalent Von Mises stresses should be below yield limit. To get an accurate representation of the stresses in critical components, frictional losses in the system are calculated. Friction causes increased loads, thus higher stresses in components. For every critical component the efficiency and Von Mises stress will be presented to verify that stresses do not exceed the yield limit and the components will not fail. The performed calculations can be found in appendix C. Materials constants such as friction coefficients and yield strengths were found in CES EduPack [31], unless mentioned otherwise.

4.2.1 Bevel Gear Assembly

The gear assembly suits two purposes. It changes the direction of rotation, and generates the speed difference required for the differential thread. Using equation 3 it was chosen to use 25 teeth on the drive gear, 28 teeth on the lead gear, and 29 on the lag gear. With this ratio the same teeth do not always match up, distributing wear along all teeth [30].

The module of the drive gear and lead is 0.8 and diameters were matched accordingly. To accommodate for the mismatching of the lag gear module, tooth shape and spacing were slightly altered. This resulted in the loss of some properties of a proper involute gear profile. The line of action is not constant, which will cause minor fluctuations in feed and thrust, which the components are able to withstand.

The bevel gears are custom made for the SFADA using 3D-printing. This greatly extended the range of possible gear parameters. Low material friction values, but high yield strength were desired, therefore the gears were made out of PLA. Surface quality from 3D-printing is limited, which increases sliding friction in the gears [32]. Based on the static friction coefficient, an efficiency of 83% was found.

The lead gear will be subject to high torques, since it is loaded with both the drilling torque as the torque required to generate thrust. Calculating the equivalent Von Mises stress at the root of the lead gear tooth gives 34 MPa. The mechanical behaviour of polymers can not be described by a constant yield limit. The average yield strength for 3D-printed PLA is 62 MPa [33]. This shows that material stresses are only slightly below material limit.

4.2.2 Thread and Screw

The threaded tube and drive screw are the components that make up the differential thread assembly. The speed difference generated in the gears is converted to a translation of the drive screw via this subassembly. A M12 thread is cut in the tube and screw. It has a lead of 1.75 mm and a diameter of 12 mm. The threaded tube is made out of POM. A large part of the SFADA's volume is taken by the threaded tube. Therefore, the use of a plastic material reduces interference in X-ray imaging. POM is well machinable, does not take on moisture and has a higher yield strength than similar materials like Nylon. The drive screw is made from steel. In order to reduce friction in the thread, the thread and screw should be from different materials. For a friction angle ϕ of 0.15 rad, and a lead angle λ of 0.04, the thread efficiency is 18%.

$$\eta_{thread} = \frac{tan\,(\lambda + \phi)}{tan\,(\lambda)} \tag{5}$$

Stresses in the thread can be calculated by combining both the contributions of shear and normal stress. Calculating the equivalent Von Mises stress gives a value of 43 kPa, well below the yield limit of 1051 MPa for steel. Similar to PLA, POM does not have a constant yield strength, but ranges between 48-72 MPa. Calculated material stresses of 22 kPa are below the yield limit.

4.2.3 Slotted Tube and Pin

Transferring torque from the lead gear to the drive screw is done by the slotted tube and pin.

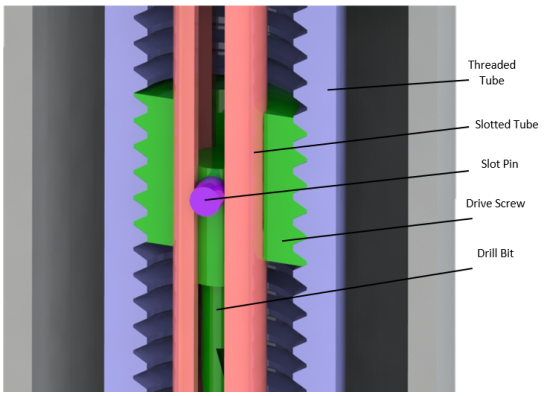

Figure 7: Close-up section view of the slot pin in the slotted tube

The combination of these components act as a straight line guide. Important aspects to the components design are the tube and slot dimension. The slotted tube has outer dimensions of 6mm, and inner of 4mm. The inside diameter matches the outer diameter of the drill bit in order to guide the drill bit. The drive pin is 1.5 mm in diameter and has a circular shape. The slot on the tube has a width that fits the pin diameter.

The tube is made from brass because of its low friction coefficient. The slot is cut using a slotting saw on a milling machine, to ensure cenctricity of the slot. The pin made of steel. Friction in the slot will cause an axial force opposing the sliding motion. This needs to be counteracted by the drive screw, thus adding to the thrust load. The efficiency of the slotted tube is 55%, which means that percentage of slotted tube torque eventually gets converted to thrust.

The total torque that the slotted tube is subject to, will cause torsion in the shaft. With the addition of the slot, torsional stiffness is reduced, increasing stresses in the material. Using Roarke's formula for slotted profiles [34] the equivalent Von Mises strength was calculated to be 69 MPa, which is below brass's yield strength of 135 MPa.

The load force and torque will be directly transferred to the slot pin, which will cause bend-

ing and shear stresses. The combination of the gives an equivalent von Mises stress of 176 MPa, below the yield strength of 1041 MPa.

4.3 System Performance

All component materials, dimensions, stresses and efficiencies contribute to the overall system performance of the SFADA. This section discusses in what way individual component performances contributes to overall performance. Using this knowledge there will be verified whether the design can theoretically achieve functional requirements. The following subsection will discuss how the losses and stresses on a component level influence the performance of the SFADA as a complete system.

The SFADA is able to generate a coupled motion from a rotational input. Rotational power at the input is converted into both rotation and translation at the output. In a system with no losses, all the power that the drill exerts is applied to the bone. The following equation displays the relation between the frictionless power and actual power as the SFADA's efficiency. The derivation of the input torque T_{in} can be found in appendix B.

$$\eta = \frac{T_{load}\omega_{drill} + \nu_{feed}F_{load}}{T_{in}\omega_{in}} \tag{6}$$

In this equation Tω is the rotational power, and νF the translational power. It was found that theoretical required power at maximum drilling loads is 31 W. From the 31 W, only 0.1% is used to generate translation. Because of this, frictional losses in the conversion of rotation of translation will only account for a very small part of the total efficiency. This shows system efficiency is not only a function of friction coefficients and dimensions, but also of the ratio between load torque and force. This can be seen in the following equation, where f_{rot} is the fraction of theoretical power required to generate rotation and f_{trans} is this for translation.

$$\frac{1}{\eta} = \frac{f_{rot}}{\eta_{rot}} + \frac{f_{trans}}{\eta_{trans}} \tag{7}$$

Losses in the translational power comprise of gear, slot and thread. This combined translational efficiency η_{trans} is 8%. This is very low with respect to rotational efficiency η_{trans} of 86%, which only consists of frictional losses in the gear. However, due to the ratio between rotational and translation power, the overall system efficiency η is 83%. For the overall device this means that at maximum load drilling, power usage is increased by 20% compared to conventional drilling. This only applicable if the surgeon is able to apply ideal drilling at constant variables, which is unlikely.

The frictional losses increase stresses in components of the SFADA. The analytical stress calculations in the previous section shows all material stresses below yield, with gear stresses approaching its limits. A finite element analysis (FEA) is done to verify this assumption. The FEA shows even higher stresses, due to concentrations as a result of the geometry. Stresses at the base of the lead gear tooth of 56 MPa are found, which is even closer to the yield strength. This means that operating at max load is likely to cause failure. To prevent this form occurring, lubrication is applied, to reduce stresses in the lead gear teeth below material limit. This enables drilling at required loads. An overview of the Finite Element analysis can be found in appendix D.

The differential thread principle of the SFADA couples rotational speed and feed. This coupling is dependent on thread and gear parameters. The chosen parameters should satisfy equation 3 to meet the requirements. For the chosen lead L of 1.75 mm, N_{lag} of 29 and N_{lead} of 28 the equation is satisfied.

The aim of the described analysis was to analytically verify the design can satisfy functional requirements During the design process user needs were taken into consideration. The analysis displayed in this chapter concludes that the design of the SFADA satisfies the functional requirements. The loads of 0.2 Nm and 20 N do not cause failure of the device, and thread and gear parameters allow for a coupled speed and feed of 1500 rpm and 1.5 mm/s. The design

Figure 8: The fabricated demonstrator of the SFADA

of the device is 80x40x36 mm, conform the requirements. A demonstrator was built according to the design, which can be seen in figure 8. Measurements have to be performed to verify whether the physical system performs as theoretically is expected.

5 Design Verification

The following section will describe the method and results of design verification. Measurements were performed using the SFADA demonstrator. This section will describe two experiments: a speed ratio measurement, and a load measurement. The first measurement is aimed to determine whether the desired ratio between feed and rotational speed can be reached. The goal of the load test is to verify that the attachment can withstand the loads experience during optimal bone drilling. For each measurement the setup and result will be presented.

5.1 Speed Ratio Measurement

There is a constant factor relating the rotational speed to feed. This factor can be considered as the effective lead. It is desired that the effective lead meets the 60 μm, which was initially considered not feasible from a single cut thread in section 2. Measurements were performed to verify that the effective lead corresponds to the desired value.

The SFADA is connected to a drill. At the initial position, with the drill bit slightly sticking out of the case, the stroke x_0 is measured . A line is fixed to the driving shaft of the SFADA. This driving shaft is rotated a number of times using the drill. This causes further protrusion of the drill bit, and coiling of the line onto the drive shaft. At the new position another measurement is made, both of the drill bit stroke x_1 and the length of the line l that has coiled up on the drive shaft. By using the following equation, the measured instances can be converted to the ratio between feed and speed. For the given shaft diameter d there is found that the effective lead L_{eff} is 61 μm. The measurement data can be found in appendix E.

$$L_{eff} = \frac{(x_1 - x_0)\pi d}{l} \tag{8}$$

5.2 Load Measurement

To display the SFADA's ability to perform a drilling procedure, a load test is done. Drilling is performed on spruce wooden samples as a bone substitute. Load forces and torques are recorded using the following setup: The SFADA is fixed above a drilling sample, with no physical connection between the two. The drilling sample is fixed to an ATI mini 40 force/torque sensor, to measure the applied load force and torque. Driving the SFADA's input shaft rotates the drill bit and slowly feeds it into the sample, which leads to a hole being drilled. After zeroing the sensor, drilling is initiated. Data recorded during drilling is led into a transducer, which transfers the signal to a data acquisition (DAQ) device. Here data is converted to a signal suitable for USB-readout.

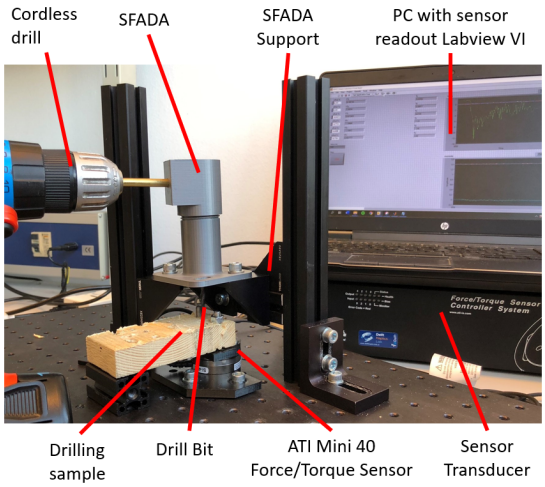

Figure 9: Overview of force/torque measurement setup

A custom LabView VI displays and saves data to the computer. The test setup can be seen in figure 9.

The drilling was performed using spruce wooden samples as a bone substitute. The SFADA was able to drill holes in several wooden samples. A plot of the recorded forces and torques can be found in figure 10. This plot displays maximum force values of 26 N and torques of 0.1 Nm. Both the thrust as the torque signal show strong vibrations. Multiple drilling tests were performed with similar results, they can be found in appendix E

The maximum torque encountered during drilling in the wooden samples was below the value required for bone drilling. To account for this, additional tests were performed. A substitute load was used in the form of a helical spring. The spring was fixed between the force/torque sensor and a custom drill bit. Due to fixation, it could apply both torque and force load. The spring was preloaded until the desired thrust of 20 N was reached. From this point onward the device is slowly actuated, with the spring counteracting both the rotation and translation of the drill bit. Maximum force and torque recorded are 22 N and 0.22 Nm respectively.

6 Discussion

Orthopaedic bone drilling has increased difficulty at hard to reach sites. The tight spaces over the bone impede the surgeon in optimal performance of the procedure. This increases the risk of complications such as thermonecrosis, crack formation, drill bit breakage and overshoot into soft tissue. Prior research has shown that a fixed drill position, a steady feed and depth control reduces this risk [19]. Conventional drilling methods do not allow for this and devices found in literature do not fit the confined volume [12, 18, 20, 21]

Therefore, a novel drilling procedure is proposed, where drilling is done using a compact self-feeding angled drill attachment (SFADA). The attachment is positioned and fixed at the bone site. A cordless drill can be held externally and angled with respect to drilling direction. Driving the SFADA generates self-feeding drilling, where the drill bit is automatically rotated and fed into the bone at the same time. When the surgeon feels and hears that the end of the bone is reached, they cease drilling. The goal of the SFADA's controlled feed and fixed position is to reduce complications when drilling in a tight space.

The project described in this report was the design of the SFADA. The following section will evaluate the design process. Following this future work will be discussed.

6.1 Design Process Evaluation

Four mechanisms were considered to generate angled self-feeding motion. Key factors in the choice for a differential thread driven device were its ability to withstand required loads and the reversibility. The speed differential was generated using a lead/lag bevel gear set. The proof of concept test showed the advantage it had over the cycloid, namely the manufactarability of the components and no wobble around the drill axis.

Choices made during the design were done with the user needs in consideration. The majority of the SFADA's volume is made from plas-

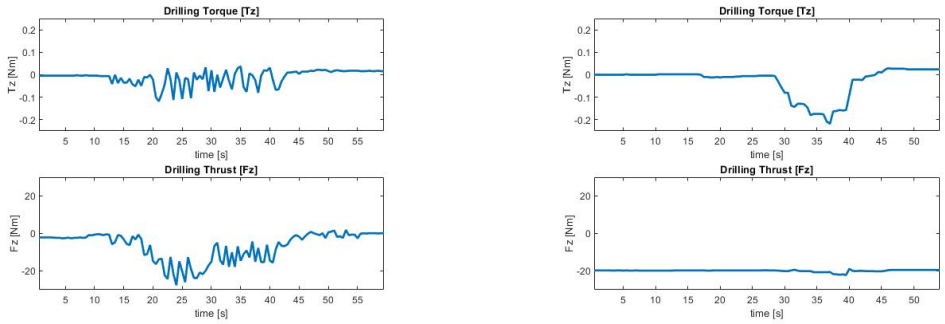

(a) Spruce wooden drilling sample

(b) Substitute drilling sample

Figure 10: Force/Torque data measured using the load test setup

tics besides the shafts, drill bit and bearings. This causes limited obstruction of X-ray imaging. When the input rotation is stopped, the device comes to an immediate standstill. This allows for safe intervention when needed. The device was chosen to be disposable, since contamination can remain present in small spaces such as the thread and gears. The low material cost on most of the components make this economically feasible. The bayonet lock allows for easy removal of drill bit when required.

A demonstrator was built according to the design. The choice was made to fabricate custom components for the device, including the gears and threads, using resources available at the TU Delft. This allowed for rapid demonstrator fabrication and quick component iterations, especially of the custom bevel gears. However, problems did arise in the gears. Stresses in the lead gear were expected to be at material limit. A lubricant was applied to reduce thread and slotted tube friction, and decrease gear stresses. As a result of this the gear did not fail, but lubricant would not be desired that close to the human body. The fluids present at the drilling site can cause the lubrication to wash out and contaminate the drilling area. In further iterations of the device it is desired to produce the gears at increased surface finish and a stronger material, such as Nylon.

The combination of a lead/lag bevel gear set with differential thread mechanism was chosen to generate the required rotational speed of 1500 rpm with a controlled feed of 1.5 mm/s. Measurement on the relation between speed and feed gave an effective lead of 61 μm. This deviates slightly from the required value of 60 μm. The deviation is very small, and likely a result of a measurement error. Based on this can be concluded that the desired speed ratio is obtained and drilling can be performed at required feed and speed.

Load measurements performed display the SFADA's ability to drill holes in spruce wooden drill samples. The measured drilling loads of the wooden drill samples, as found in figure 10, show lower loads than those expected during bone drilling. Therefore, additional testing was done under substitute loads. These tests show that the device can transfer loads up to 22 N and 0.22 Nm. This satisfied the required values of 20 N and 0.2 Nm. No bone drilling test where performed, since this material was not allowed in the labs.

Despite the loads being equal to optimal bone drilling, there can not be concluded that the SFADA is able to perform drilling in bone. Where during the conventional procedure the drill is initially at standstill, and from there slowly fed into the bone, the SFADA approaches the bone with an initial speed. This can cause forces and torques to temporarily exceed expected values upon penetration of the bone. Load measurements in the wooden sample display this phenomena, as can be seen in figure 10 and appendix E. An initial in-

crease upon penetration in thrust can be distinguished. The thrust reduces to a steady value once the drill is has fully entered the wood. The increased loads can cause the device to fail. Further work needs to be done to verify device functioning during a bone drilling procedure.

The novel ability to apply a controlled feed in a tight space is a key component to improving bone drilling at hard to reach bone sites. No instance found in literature has displayed these abilities. This shows that the device presented in this report is the first instance of a compact angular self-feeding drilling attachment. The design meets all requirements needed for optimal bone drilling, but further work needs to be done to verify this.

6.2 Future Work

With the SFADA being a key part of the novel bone drilling procedure, further work is needed to develop the complete drilling system.

Bone drilling tests need to be performed. Earlier measurements done using substitute loads show promising results, but do not verify the SFADA's ability to perform bone drilling. The novel drilling procedure can cause forces and loads to increase upon penetration of the bone, which might cause the device to fail. A load measurement during bone drilling is desired.

In order to prevent the SFADA from pushing itself away from the bone when drilling, a mechanism is required that fixes the device to the drilling site. Research is required to gain an insight into methods of fixation and acquire a set of device specifications.

The controlled application of feed introduced by the SFADA reduces risk of overshoot, because the feed is controlled by the rotation, and not dependent on resistance encountered by the drill. This requires the user to pay attention to a change in torque or sound by the drill. To aid the user a breakthrough detection mechanism could be implemented. This is to automatically detect the end of the bone when drilling. The addition of a sensor would be necessary to gain insight into drilling torque, and an algorithm is required to convert this data to breakthrough detection mechanism.

In the continuation of the project, the design should be validated with the surgeon. Tests should be performed that resemble the actual bone drilling procedure, or even perform trials in the cutting room.

7 Conclusion

Orthopaedic drilling at hard to reach bone sites has an increased risk of complications. To reduce this risk, a novel procedure was proposed. Drilling should be done using the Self-Feeding Angled Drill Attachment (SFADA). The SFADA introduces a newfound level of control to the procedure. The controllable feed can apply optimal drilling conditions and prevent that the drill bit overshoots the bone. These functionalities combined in a compact design allow for performance at hard to reach bone sites which has not been possible yet. Further work needs to be done to verify the reduction of complications during bone drilling, but the SFADA design presented in this report is a key component of the improved procedure.

Acknowledgements

The author would like to thank people involved during this project. This thesis report is part of a running project, initiated by L. Krijgsman. His research and results have been of great value to the project. Secondly the author would like to thank traumasurgeons K.A. Bartlema M.D. and M. van der Elst M.D. Their experiences and expertise introduced the problem of drilling at hard to reach bone sites and provided boundaries and guidelines during the design. Dr. van der Elst also provided the opportunity to spend several days observing drilling procedures in the operation room, which helped gain useful insights. Finally the author would like to thank J.W. Spronck, the supervisor of the project. The discussions and meetings filled with endless creativity and energy have been very stimulating and motivating over the dura-

tion of the project.

References

[1] M. L. Routt and P. T. Simonian, "Internal fixation of pelvic ring disruptions," *Injury*, vol. 27, no. SUPPL. 2, pp. 20–30, 1996.

[2] M. E. Müller, M. Allgöwer, M. E. Müller, R. Schneider, and H. Willenegger, *Manual of internal fixation: techniques recommended by the AO-ASIF group*. Springer Science & Business Media, 1991.

[3] N. Bertollo and W. Robert, "Drilling of Bone: Practicality, Limitations and Complications Associated with Surgical Drill-Bits," *Biomechanics in Applications*, 2011.

[4] D. A. Wong, J. H. Herndon, S. T. Canale, R. L. Brooks, T. R. Hunt, H. R. Epps, S. S. Fountain, S. A. Albanese, and N. A. Johanson, "Medical errors in orthopaedics results of an AAOS member survey," *Journal of Bone and Joint Surgery - Series A*, vol. 91, no. 3, pp. 547–557, 2009.

[5] Y. Zhang, L. Xu, C. Wang, Z. Chen, S. Han, B. Chen, and J. Chen, "Mechanical and thermal damage in cortical bone drilling in vivo," *Proceedings of the Institution of Mechanical Engineers, Part H: Journal of Engineering in Medicine*, vol. 233, no. 6, pp. 621–635, 2019.

[6] G. Augustin, T. Zigman, S. Davila, T. Udilljak, T. Staroveski, D. Brezak, and S. Babic, "Cortical bone drilling and thermal osteonecrosis," 2012.

[7] G. Singh, V. Jain, and D. Gupta, "Comparative study for surface topography of bone drilling using conventional drilling and loose abrasive machining," *Proceedings of the Institution of Mechanical Engineers, Part H: Journal of Engineering in Medicine*, vol. 229, no. 3, pp. 225–231, 2015.

[8] Y. Wang, M. Cao, Y. Zhao, G. Zhou, W. Liu, and D. Li, "Experimental investigations on microcracks in vibrational and conventional drilling of cortical bone," *Journal of Nanomaterials*, vol. 2013, 2013.

[9] M. V. Price, S. Molloy, M. C. Solan, A. Sutton, and D. M. Ricketts, "The rate of instrument breakage during orthopaedic procedures," *International Orthopaedics*, vol. 26, no. 3, pp. 185–187, 2002.

[10] H. Clement, N. Heidari, W. Grechenig, A. M. Weinberg, and W. Pichler, "Drilling, not a benign procedure: Laboratory simulation of true drilling depth," *Injury*, vol. 43, no. 6, pp. 950–952, 2012.

[11] M. Cevzar, T. Petrič, and J. Babič, *Advances in Service and Industrial Robotics*, vol. 49. 2018.

[12] B. Allotta, G. Giacalone, and L. Rinaldi, "A hand-held drilling tool for orthopedic surgery," *IEEE/ASME Transactions on Mechatronics*, vol. 2, no. 4, pp. 218–229, 1997.

[13] L. Kudla, "Influence of feed motion features on small holes drilling process," *Journal of Materials Processing Technology*, vol. 109, no. 3, pp. 236–241, 2001.

[14] G. P. Moustris, S. C. Hiridis, K. Deliparaschos, and K. Konstantinidis, "Visual servoing in medical robotics: a survey. Part I: endoscopic and direct vision imaging – techniques and applications Mahdi," *The international journal of medical robotics + computer assisted surgery : MRCAS*, vol. 7, no. April, pp. 375–392, 2011.

[15] D. Baker, P. N. Brett, M. V. Griffiths, and L. Reyes, "A mechatronic drilling tool for ear surgery: A case study of some design characteristics," *Mechatronics*, vol. 6, no. 4 SPEC. ISS., pp. 461–477, 1996.

[16] W. Gregoor, "Hydropowered minimally invasive surgical bone drill," tech. rep., TU Delft, 2015.

[17] L. Krijgsman, "The Design of a Compact Angular Drilling Device for Medical Application," tech. rep., TU Delft, 2019.

[18] S. Shim, H. Choi, D. Ji, W. Kang, and J. Hong, "Robotic System for Bone Drilling Using a Rolling Friction Mechanism," *IEEE/ASME Transactions on Mechatronics*, vol. 23, no. 5, pp. 2295–2305, 2018.

[19] C. J. Walsh, A. J. Meskers, A. H. Slocum, and R. Gupta, "CT-Compatible Medical Drilling Stylet," *Journal of Medical Devices, Transactions of the ASME*, vol. 6, no. 4, pp. 1–8, 2012.

[20] T. Boiadjiev, G. Boiadjiev, K. Delchev, K. Zagurski, and R. Kastelov, "Far cortex automatic detection aimed for partial or full bone drilling by a robot system in orthopaedic surgery," *Biotechnology and Biotechnological Equipment*, vol. 31, no. 1, pp. 200–205, 2017.

[21] M. Louredo, I. Díaz, and J. J. Gil, "DRIBON: A mechatronic bone drilling tool," *Mechatronics*, vol. 22, no. 8, pp. 1060–1066, 2012.

[22] P. N. Brett, D. A. Baker, L. Reyes, and J. Blanshard, "An automatic technique for micro-drilling a stapedotomy in the flexible stapes footplate," *Proceedings of the Institution of Mechanical Engineers, Part H: Journal of Engineering in Medicine*, vol. 209, no. 4, pp. 255–262, 1995.

[23] F. R. Ong and K. Bouazza-Marouf, "Detection of drill bit break-through for the enhancement of safety in mechatronic assisted orthopaedic drilling," *Mechatronics*, vol. 9, no. 6, pp. 565–588, 1999.

[24] Y. Torun, A. Ozturk, N. Hatipoglu, and Z. Oztemur, "Breakthrough detection for orthopedic bone drilling via power spectral density estimation of acoustic emission," in *2018 Electric Electronics, Computer Science, Biomedical Engineerings' Meeting, EBBT 2018*, pp. 1–5, 2018.

[25] Y. L. Hsu, S. T. Lee, and H. W. Lin, "A modular mechatronic system for automatic bone drilling," *Biomedical Engineering - Applications, Basis and Communications*, vol. 13, no. 4, pp. 168–174, 2001.

[26] M. Hessinger, J. Hielscher, P. P. Pott, and R. Werthschutzky, "Handheld surgical drill with integrated thrust force recognition," in *2013 E-Health and Bioengineering Conference, EHB 2013*, pp. 1–4, IEEE, 2013.

[27] M. Hessinger, M. Pingsmann, J. C. Perry, R. Werthschutzky, and M. Kupnik, "Hybrid position/force control of an upper-limb exoskeleton for assisted drilling," in *IEEE International Conference on Intelligent Robots and Systems*, vol. 2017-Septe, pp. 1824–1829, 2017.

[28] A. Bhatia, *Basic Fundamentals of Gear Drives*. No. 877.

[29] M. Blagojevic, N. Marjanovic, B. Stojanovic, and L. Ivanovic, "Influence of the friction on the cycloidal speed reducer efficiency," no. May 2014, 2012.

[30] A. Arbor and C. R. Mischke, *Standard Handbook of Machine Design*. 1996.

[31] Granta Design Limited, "CES Edupack Software," 2009.

[32] W. Pawlak, "Wear and coefficient of friction of PLA - Graphite composite in 3D printing," no. May, 2018.

[33] S. M. Lebedev, O. S. Gefle, E. T. Amitov, D. V. Zhuravlev, D. Y. Berchuk, and E. A. Mikutskiy, "Mechanical properties of PLA-based composites for fused deposition modeling technology," *International Journal of Advanced Manufacturing Technology*, vol. 97, no. 1-4, pp. 511–518, 2018.

[34] W. C. Young and R. G. Budynas, *Roark ' s Formulas for Stress and Strain*. 2001.

A Self Feeding Concept Development

Several concepts were considered to generate the self-feeding motion. The concepts described in this section are adaptions of previous designs. Firstly, the criteria will be discussed that determine the feasibility of the design. These criteria are based on the functional requirements and user needs. The criteria describe whether the design specifications are obtainable for the given concept. Secondly, the concepts will be introduced. A brief description of their working principle is given. The concepts will be evaluated with regards to the criteria. Concluding an overview is presented of the concepts in a decision-matrix. Scores will be assigned to each criteria and the most feasible concept selected.

A.1 Concept Criteria

The origin of all concept criteria will be discussed in this section. They describe the ability of a design to meet functional requirements and user needs.

No slip

Slipping of components can compromise several features of the design. It stops the ability to correctly transfer loads to the bone. The cordless drill might be rotating, but the drill bit could be at standstill. This does not guarantee proper functioning, and the prevention of complications.

No Jamming

Form-fitting mechanism allow for a controlled and predictable transfer of motion and force between components. However, when one of the components is slightly deformed, jamming can occur. Since drilling will be done using a conventional power drill, jamming will increase drill torque until a component breaks. Therefore the risk of jamming should be minimized.

Required Loads

To perform optimal bone drilling, the device should meet the loads experienced during drilling. The device should have sufficient strength in the loading direction to ensure that it meets the requirements.

Reverse

In order to retrieve the drill bit form the bone site during a drilling procedure, the device should be able to retract the drill bit. This has to be performed by simply reversing direction on the cordless drill. By this the procedure will remain intuitive to the user.

Sensing Interference

During the current drilling procedure, the surgeon ceases drilling when they feel and hear that the end of the bone is reached. The surgeons experience allows him to perform this accurately. The novel procedure uses the sample principle, so the device should not interfere with this. Additional forces or sounds in the device prevent the surgeon from hearing and feeling the end of the bone.

Manufacturability

As mentioned, the design will be made at the TU Delft. This means that using the resources available, the manufacturing of a demonstrator should be obtainable. Complex component in a design are not favourable for this criterion.

A.2 Self-feeding Concepts

Multiple concepts were considered towards the development of a self-feeding drill attachment. The following subsection discusses possible mechanism concepts. Additionally, the concepts will be evaluated based on the criteria.

Angled Friction Wheel

The friction wheel concept has a driven shaft with angled rollers connected to it. Rotating the rollers result in a force on the shaft that generates both rotation and translation of the shaft. The contact force on the shaft is dependent on friction, which has a high risk of slip. It is well constrained so jamming is not likely. Maximum friction force is dependent on the preload on the shaft, which is limited. No stiffness elements are in line with the shaft, so drill torque can be sensed directly. The positioning of the rollers is crucial, and at the same time the most complex part of the design. It is manufacturable, but proper outlining of the rollers will be a challenge. Reversing motor torque would result in reverse of drill motion, making it backdrivable.

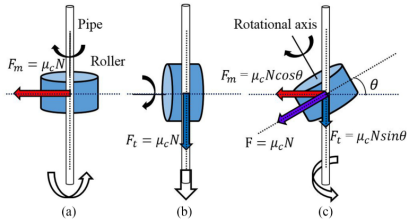

Figure 11: Description of rolling friction principle (from [167])

Flexible drive, carriage and cable

From previous research on this problem came the concept of the linear carriage drill. In this concept the the drill was externally actuated and could translate independently. Adding a pulley mechanism to this design allows for self feeding motion of the drill. Coiling of a cable onto the pulley shortens the cable and would pull the carriage. Cables can only exert forces under tension, so only pulling would be possible. To account for this a spring pushes the carriage back from lowered position. The system has no risk of slip, the mechanism is no based on friction. Jamming is likely. The three shaft design is over constrained, so slight imperfections in the shafts can cause jamming during travel. High loads are possible, but the system is limited by the tension in the cable. Cable needs to be flexible enough to coil around the pulley, but withstand high loads. The spring element in series with the drilling force will interfere with the surgeons ability to sense the end of the bone. The system is relatively simple and is already shown to be manufacturable. The system is not backdrivable. With the spring it auto retracts, but a protruded cannot be held.

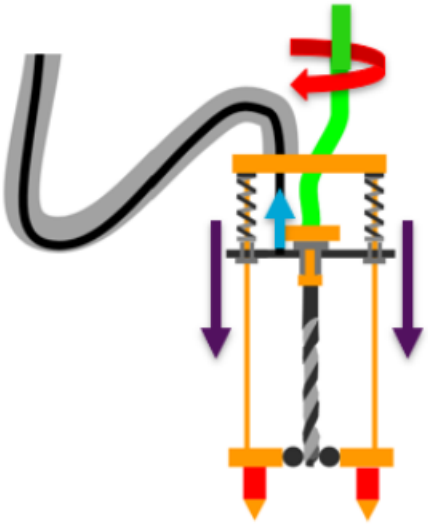

Figure 12: Description of design by Krijgsman [17], the addition of a pulley mechanism would generate self-feeding

Thread and gears

Lead screw mechanisms use threads to generate translation. The thread is actuated, and by constraining rotation a screw starts to translate along the thread. The thread concept uses a similar approach, but requires both rotation and translation of the outgoing shaft. This is done by also rotating the screw, but at a different speed. Threads are form fitting, so not entirely dependent on friction. Slip is not a risk in this system, but jamming is. The transmission comprises of bevel gears. Deformations of the gears while in use can cause jamming. Threads can handle high axial loads, so the drilling loads can be countered. Sensing of the drill depth would still be possible, since the principle is familiar to conventional drilling. The combination of lead screw and bevel gear is backdrivable.

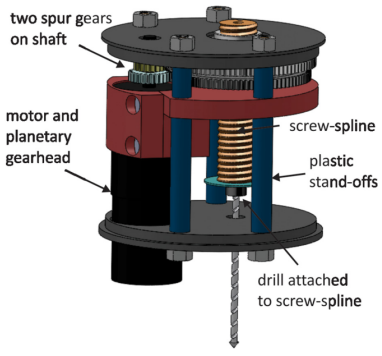

Figure 13: Thread driven design by Walsh [182]

Hydro motor and cylinder

The hydromotor concept is based on a reversed external gear pump. Applying pressure to one side of the chamber allows for rotation of the drill. The external gear assembly is free to translate since it is attached to a plunger in a cylinder. Slowly filling the cylinder results in feed travel of the drill bit. There is no risk of slipping in this concept, the working principle does not rely on friction. Jamming in the gears and cylinder would be possible due to deformations, since the design is form-fitting. Proper dimensioning of the system should reduce this. Direct sensing is not possible. A drill is connected to a pump, and the pump is connected to the hydromotor. The complete drilling principle is altered, and the surgeon will have a hard time controlling the depth. The mechanism would be very complicated to manufacture. Components in the hydromotor are very small and are under high forces. Slight imperfections or play between gears causes pressure leakage. This would cause the system to stop rotating. Using a single input flow can not reverse the direction of feed and drilling, because the system is open. The water leaves the system, so reversing does not suck it back in.

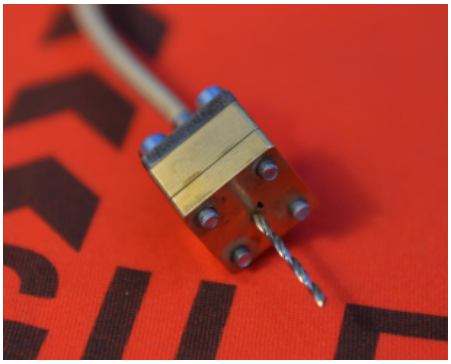

Figure 14: Hydro powered drill by Gregoor[138]

A.3 Concept Scoring

Based on the arguments displayed in the decision matrix can be concluded that the thread and gear concepts is the most feasible.

Table 3: Decision-matrix for concept selection

Concept	**A** Angled Friction Wheel	**B** Flexible drive, carriage and cable	**C** Thread and gears	**D** Hydro motor and cylinder
Required Loads	0	1	2	1
No Slip	0	2	2	2
No Jamming	2	1	1	1
Reverse	2	0	2	0
Sensing Interference	2	1	2	0
Manufacturability	1	2	2	0
Total	7	7	**11**	4

B Force and Torque Analysis

To analytically derive the forces and torques components are subject to, static analysis is performed. For every critical components a free body diagram is made. Unknown variables are identified. Force and torque equilibria are assumed and the equations are solved.

$$\omega_{in} = R_{lead}\omega_{out} \tag{9}$$

$$\omega_{in} = \frac{2\pi}{P}\frac{R_{lag}R_{lead}}{R_{lag} - R_{lead}}\nu \tag{10}$$

$$T_{in} = \eta_F \frac{r\tan\lambda(R_{lag} - R_{lead})}{R_{lag}R_{lead}}F_{load} + \eta_T \frac{1}{R_{lead}}T_{load} \tag{11}$$

$$\eta_F = \eta_{thread}\eta_{slot}\eta_{gear} \tag{12}$$

$$\eta_T = \eta_{gear} \tag{13}$$

$$\eta = \frac{T_{load}\omega_{out} + \nu_{feed}F_{thrust}}{T_{in}\omega_{in}} \tag{14}$$

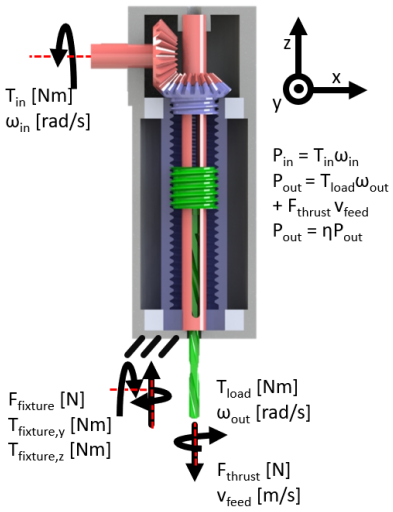

Figure 15: Free body diagram of the SFADA

Bevel Gear assembly

$$T_{in} = \frac{1}{\eta_{gear}}(\frac{T_{lead}}{R_{lead}} - \frac{T_{lag}}{R_{lag}}) \tag{15}$$

$$R_{lead} = \frac{N_{lead}}{N_{in}} \tag{16}$$

$$R_{lag} = \frac{N_{lag}}{N_{in}} \tag{17}$$

$$\eta_{gear} = \frac{\tan\alpha}{\tan\alpha + \arctan\mu_{gear}} \tag{18}$$

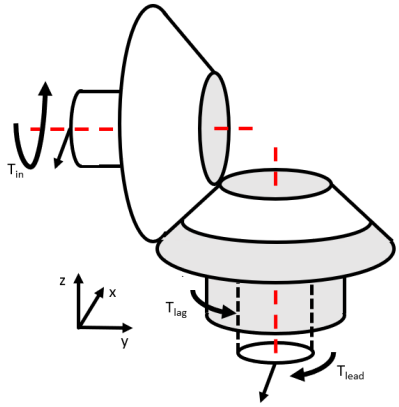

Figure 16: Free body diagram of the bevel gear assembly

Slotted Tube

$$\sum M_z = 0; T_{lead} - F_{slot}d_{st} = 0 \tag{19}$$

$$\sum F_z = 0; F_{z,lead} - 2F_{w,slot} = 0 \tag{20}$$

$$F_{w,slot} = \mu_{slot}F_{slot} \tag{21}$$

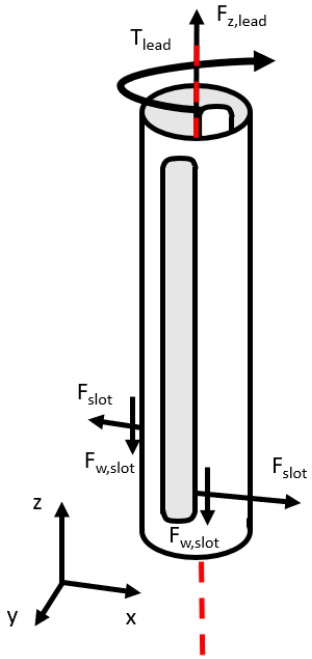

Figure 17: Free body diagram of the slotted tube

Slot Pin

$$\sum F_z = 0; F_{z,load} + 2F_{w,slot} - F_{z,pin} = 0 \tag{22}$$

$$\sum M_z = 0; T_{load} + T_{lower} + F_{slot} d_{slot} = 0 \tag{23}$$

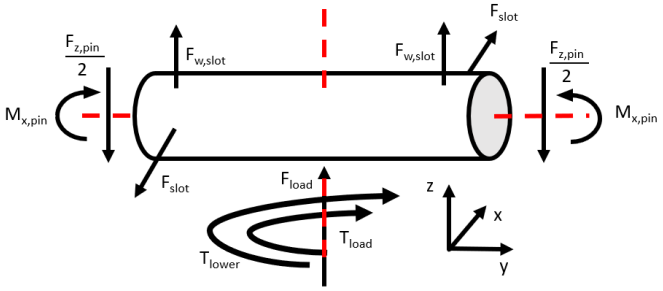

Figure 18: Free body diagram of the slot pin

Drive Screw

$$\sum M_z = 0; T_{load} r_{screw} - \sin\lambda F_{n,thread} - \cos\lambda F_{w,n,thread} = 0 \tag{24}$$

$$\sum F_z = 0; F_{z,pin} + sin\lambda F_{w,n,thread} - cos\lambda F_{n,thread} = 0 \tag{25}$$

$$F_{w,n,thread} = \mu_{thread} F_{n,thread} \tag{26}$$

$$\eta_{thread} = \frac{\tan\lambda}{\tan\lambda + \phi} \tag{27}$$

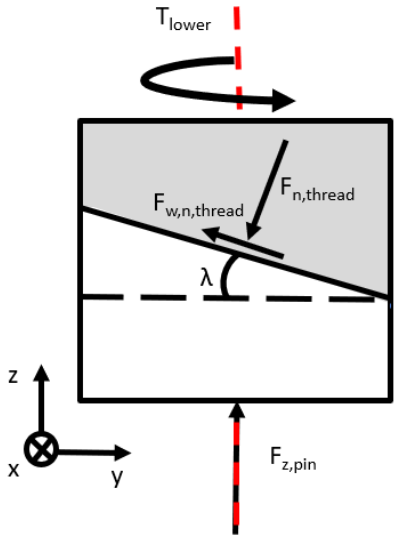

Figure 19: Free body diagram of the drive screw

C Matlab Codes

The matlab codes used to calculate device performance are included in this appendix. The first code contains all design variables that describe the device. The second code calculates forces in all relevant components of the SFADA. Based on frictional losses the efficiencies are determined. The third code uses forces in design variables and forces in components to determine material stresses. Von Mises equivalent stresses are compared to yield limits.

Final design parameters

```
%% Thread Paramters
% Consists of design choices and requirements needed for
    calculatotions on
% the design of the drill prototype

%% Requirements

rpm_drill = 1500; % Drill speed [rpm]
fr = 1.5; % [mm/s] 75 mm/min

T = 0.2; % [Nm] max torque
F = 20; % [N] max force

%% Differential Thread Variables

% Drill variables
d_drill = 4e-3;

% Drive Gear Variables
H_ds = 10e-3; % Drive screw height[m]

% Slotted Tube Variables
d_st = 6e-3; % Slotted tube diameter [m]
d_sp = 1.5e-3; % Slot pin diameter [m]

% Thread Variables
r_thr = 6e-3; % Thread Radius [m]
P = 1.75e-3; % Pitch [mm]
labda = atan(P/(r_thr*pi*2)); % Lead angle [rad]
H_thr = (sqrt(3)/2)*P;
w_thr = 2*tan(deg2rad(30))*H_thr;
l_thr = H_ds/sin(labda); % Thread surface length [m]
A_thr = sin(labda)*w_thr*l_thr; % Thread surface [m^2]

%% Bevel Gear Variables

%F_pre = 0; %  Gear shaft preload [N]
Module = 0.8; % gear module [D/N]
alpha_gear = deg2rad(20); % pressure angle [rad]
del_gear = deg2rad(45); % Taper angle [rad]
```

```
d_shaft = 6e-3; % (Drive) Shaft diameter [mm]

% Teeth numbers and gear ratios
n_in = 17; % nr of teeth on drive gear
n_lead = 28; % nr of teeth on inner gear
n_lag = 29; % nr of teeth on outer gear
R_lead = n_lead/n_in; % reduction factor from in to inner
R_lag = n_lag/n_in; % reduction factor from in to outer

% Input gear variables
M_in = Module;
d_avg_in =  M_in*1e-3*n_in;
r_avg_in = d_avg_in/2;
d_i_in = d_shaft;
d_o_in = d_avg_in*2 - d_i_in;
b_in = (d_o_in - d_i_in)/(2*cos(del_gear));
w_in = M_in/2;

% Lead gear variables
M_lead = Module;
d_avg_lead = M_lead*1e-3*n_lead; % average lead gear diamter [mm]
r_avg_lead = d_avg_lead/2; % average lead gear radius [mm]
d_i_lead = d_shaft; % lead gear inner diamter [mm]
d_o_lead = d_avg_lead*2 - d_i_lead; % lead gear outer diamter [mm]
b_lead = (d_o_lead - d_i_lead)/(2*2*cos(del_gear)); % lead gear tooth
    length [mm]
w_lead = M_lead/2; % lead gear tooth width (approx) [mm]

% Lag gear variables
M_lag = d_avg_lead*1e3/n_lag; % lag gear module
d_avg_lag = d_avg_lead; % average lag gear diamter [mm]
r_avg_lag = d_avg_lag/2; % average lag gear radius [mm]
d_i_lag = d_shaft; % lag gear inner diamter [mm]
d_o_lag = d_avg_lag*2 + d_i_lag; % lag gear outer diamter [mm]
b_lag = (d_o_lag - d_i_lag)/(2*2*cos(del_gear)); % lag gear toot
   length [mm]
w_lag = M_lag/2; % lag gear tooth width (approx) [mm]

%% Speed Variables [R = N_out/N_in = omega_in/omega_out]

omega_drill = 2*pi*rpm_drill/60; % drill velocity [rad/s]
omega_lead = omega_drill; % slotted tube velocity [rad/s]
omega_in = omega_drill*R_lead;
omega_lag = omega_in/R_lag; % threaded tube velocity [rad/s]
omega_thread = omega_lead - omega_lag; % relative velocity thread [
   rad/s]
fr_real = omega_thread*P*1000/(2*pi); % real feed speed w gears [mm/s
   ]
```

```
%% Material Properties

E_pom = 0;
E_steel = 0;
E_messing = 0;

% Thread Material Properties
E_thr = E_pom;
mu_s_thr = 0.15; % 0.1-0.15 Pom on Steel (lubricated)
mu_d_thr = 0.2; % 0.15-0.25 Pom on Steel (lubricated)
phi_thr = atan(mu_d_thr); % angle of friction

% Gear Material Properties
mu_d_gear = 0.45; % 0.38-0.45 Pla on Pla

% Slot Material Properties
mu_d_slot = 0.19; % Brass on steel (lubricated)

%% Design Rule
1 - (n_lead/n_lag)

2*pi*fr*1e-3/(P*omega_drill)

%%

omega_drill*P/(2*pi*fr*1e-3)

n_lag/(n_lag-n_lead)
```

Final design forces and efficiencies

```
%% Internal Thread Concept Loss and Force analysis

threadparams;

%% Drive Screw Forces

syms T_lead

F_f_st = mu_d_slot*T_lead/(d_st/2);

T_lower = (F + F_f_st)*r_thr*tan(labda + atan(mu_d_thr));

T_lead = double(solve(T_lead == T_lower + T, T_lead));
T_lower = double(subs(T_lower));

%% Drive Screw Efficiency

T_lower_nofric = F*r_thr*tan(labda);
T_lower_nofric_st = F*r_thr*tan(labda + atan(mu_d_thr));
```

```
%T_lower_nofric_thr = -T + ((F*r_thr*tan(labda) + ...
%    T)/(1-(2*mu_d_slot/d_st)*r_thr*tan(labda)) )

%eff_thr = T_lower_nofric/T_lower_nofric_st
%eff_st = T_lower_nofric/T_lower_nofric_thr % GIVES STRANGE VALUES
eff_thr_st = T_lower_nofric/T_lower


%% Gear Forces
% NOTE DAT KRACHT OP INKOMENDE GEAR ALLEEN AFHANKELIJK IS VAN LOAD
    TORQUE

T_lag = T_lower;

F_lead = (T_lead/r_avg_lead)/(1-mu_d_gear*tan(alpha_gear));
F_lag = (T_lag/(r_avg_in*R_lag))/(1-mu_d_gear*tan(alpha_gear));

T_in = (F_lead-F_lag)*r_avg_in

%% Gear Efficiency

T_in_nofric = (T_lead/R_lead) - (T_lag/R_lag);

eff_gear = T_in_nofric/T_in

%% Total Efficiency

T_in_nofric = (F*(P*r_thr*(R_lag-R_lead)/(2*pi*r_thr*R_lag*R_lead)) +
    ...
    T*(1/(R_lead)));

eff_totalA = T_in_nofric/T_in
```

Final design stresses

```
%% Internal Thread Concept Failure Analysis

clear all;
clc;

thread_forces;

%% Slotted Tube Torsional Shear
% From table 10.1 -> 27 Roark's Formulas for stress and strain

ri = d_drill/2;
ro = d_st/2;
h = d_sp;

ri_ro = ri/ro;
```

```
h_ri = h/ri;

K1 = 2.0014 - 0.1400*h_ri - 0.3231*h_ri^3;
K2 = 2.9047 + 3.0069*h_ri - 4.05*h_ri^2;
K3 = -15.721 - 6.5077*h_ri - 12.496*h_ri^2;
K4 = 29.553 + 4.1115*h_ri + 18.845*h_ri^2;
B = K1 + K2*ri_ro + K3*ri_ro^2 + K4*ri_ro^3;
tau_max_st = T_lead*B/(ro^3);
sig_vm_st = sqrt(3*tau_max_st^2)

sig_yield_st = 135*1e6; % Yield strength brass (135 Mpa)

if(sig_vm_st < sig_yield_st)
    disp("Slotted tube stress below yield strength, NO FAILURE")
else
    disp("Slotted tube  stress exceeds yield strength, FAILURE")
end

%% Thread Torsional Shear and Axial Stress
% From paper

r_st = d_st/2;
sig_vm_thr = sqrt((F/(pi*(r_thr^2-r_st^2)))^2 + ...
    3*(2*T_lower*r_thr/(pi*(r_thr^4-r_st^4)))^2)

sig_yield_thr = 350*1e6; % Yield strength steel (350 Mpa)

if(sig_vm_thr < sig_yield_thr)
    disp("Drive screw stress below yield strength, NO FAILURE")
else
    disp("Drive screw stress exceeds yield strength, FAILURE")
end

r_o_thr = 18e-3;

sig_vm_thrtube = sqrt((F/(pi*(r_o_thr^2-r_thr^2)))^2 + ...
    3*(2*T_lower*r_thr/(pi*(r_o_thr^4-r_thr^4)))^2)

sig_yield_thrtube = 69*1e6; % Tensile strength POM (69 Mpa)

if(sig_vm_thrtube < sig_yield_thrtube)
    disp("Threaded tube stress below yield strength, NO FAILURE")
else
    disp("Threaded tube stress exceeds yield strength, FAILURE")
end



%% Slot Pin Force Shear (Updated 25-3)
```

```
% y is in dir of pin (axial)
% z is in dir of drill bit (radial)
% x is other dir (radial)

%V_xz_sp_max = F/2; % Max shear force as a result of F_load
%M_x_sp_max = F*(d_st/8); % Max bending moment as a result of F_load
%M_z_sp_max = T;

V_max_sp = (3/2)*(T/d_drill);

sig_yz_sp = 4*V_max_sp/(3*pi*((d_sp/2)^2 - (0.5*1e-3)^2));
sig_vm_sp = sqrt(3*sig_yz_sp^2)

sig_yield_sp = 1.041e+9; % yield strength spring steel (1041 Mpa);

if(sig_vm_sp < sig_yield_sp)
    disp("Slot pin stress below yield strength, NO FAILURE")
else
    disp("Slot pin stress exceeds yield strength, FAILURE")
end

%% Drive Gear Bending Stress and Force Shear

% Shear stresses on gear teeth
%F_gear = double(subs(F_t_gear));

tau_xy_in = (T/d_avg_in)/(b_in*w_in);

% Bending stress from lewis Equation
Y_gear = 0.32; % based on nr of teeth and taper angle phi [but we
    call it alpha]
sig_lewis_in = (2*T/d_avg_in)/(b_in*pi*M_in*1e-3*Y_gear);

sig_vm_in = sqrt(sig_lewis_in^2 + 3*tau_xy_in^2)

sig_yield_in = 58*1e6 % yield strength Pla (58 Mpa)

if(sig_vm_in < sig_yield_in)
    disp("Drive gear tooth stress below yield strength, NO FAILURE")
else
    disp("Drive gear tooth stress exceeds yield strength, FAILURE")
end

%% Lead Gear Bending Stress and Force Shear

% Shear stresses on gear teeth
%F_gear = double(subs(F_t_gear));
```

```
w_lead_min = d_i_lead/(2*n_lead);
tau_xy_lead = (2*T_lead/(d_i_lead+d_o_lead))/(b_lead*(w_lead-
    w_lead_min));

% Bending stress from lewis Equation
Y_gear = 0.32; % based on nr of teeth and taper angle phi [but we
    call it alpha]
M_avg_lead = d_avg_lead/n_lead;
sig_lewis_lead = (2*T_lead/(d_i_lead+d_o_lead))/(b_lead*pi*M_avg_lead
    *Y_gear);

sig_vm_lead = sqrt(sig_lewis_lead^2 + 3*tau_xy_lead^2)

sig_yield_lead = 58*1e6 % yield strength Pla (58 Mpa)

if(sig_vm_lead < sig_yield_lead)
    disp("Lead gear tooth stress below yield strength, NO FAILURE")
else
    disp("Lead gear tooth stress exceeds yield strength, FAILURE")
end
```

D Finite Element Analysis Results

The following appendix displays the results from the Finite Element Analysis. For every critical component equivalent Von Mises stresses are calculated, and the maximum value is highlighted.

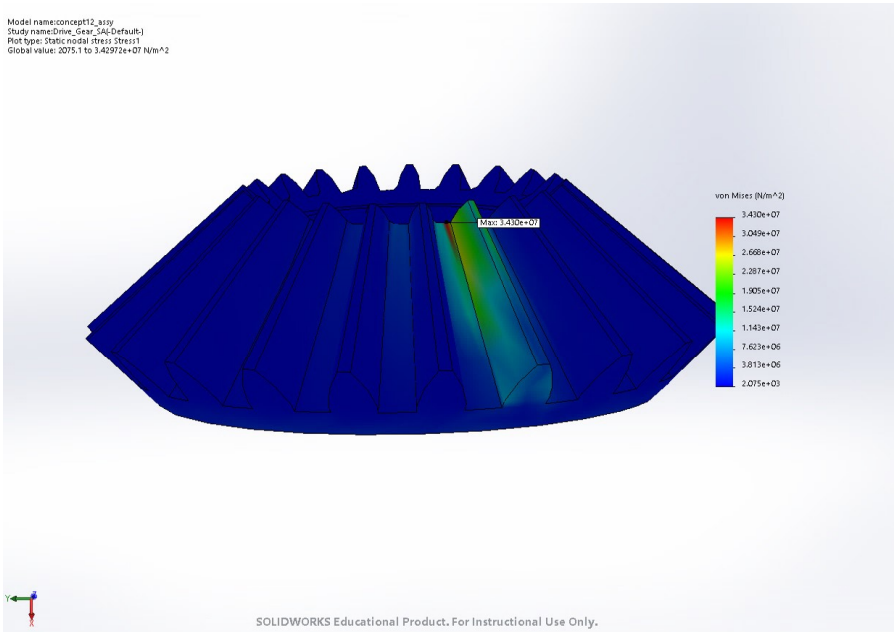

Figure 20: Drive gear FEA, with a maximum Von Mises stress of 34 MPa

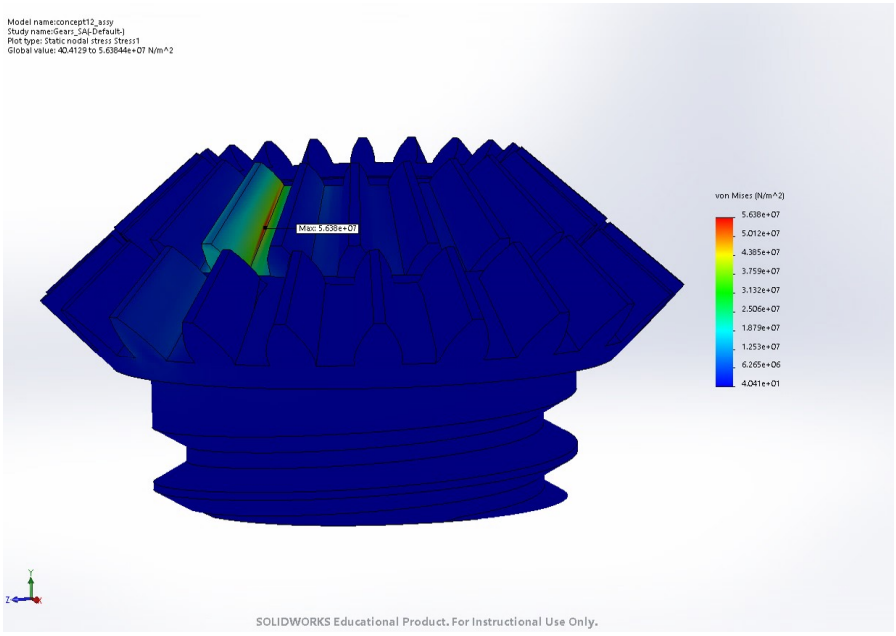

Figure 21: Lead/lag gear FEA, with a maximum Von Mises stress of 56 MPa

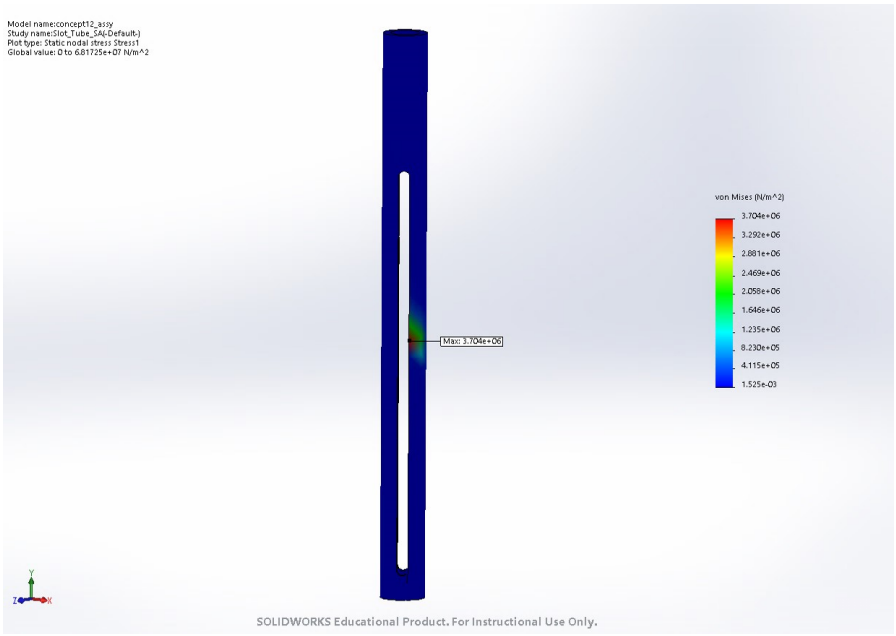

Figure 22: Slotted tube FEA, with a maximum Von Mises stress of 3.7 MPa

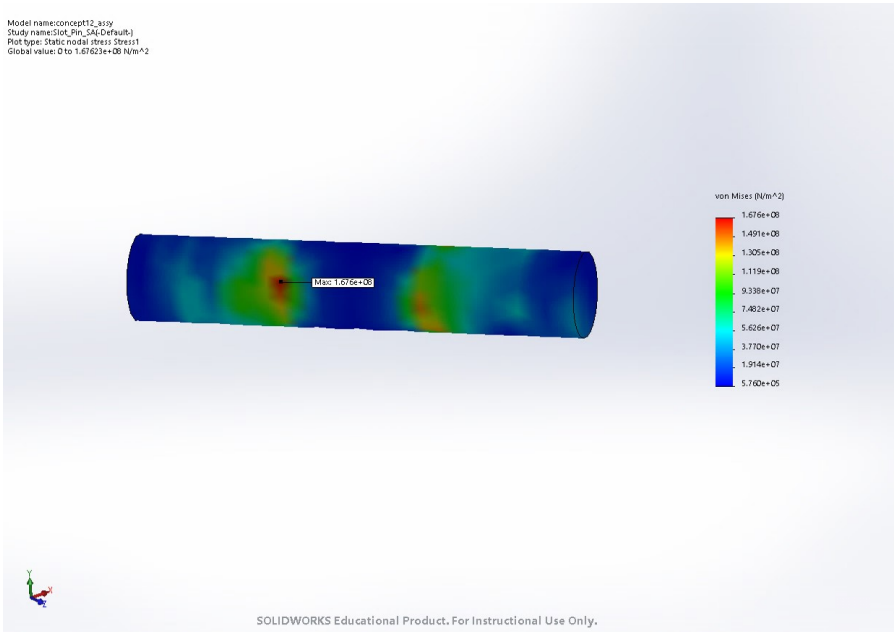

Figure 23: Slot pin FEA, with a maximum Von Mises stress of 167 MPa

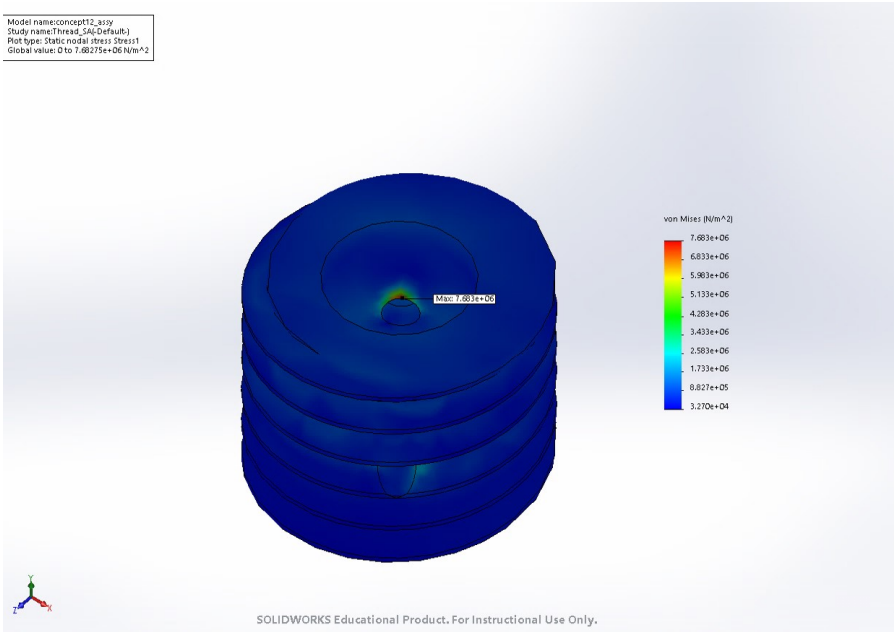

Figure 24: Drive screw FEA, with a maximum Von Mises stress of 7.7 MPa

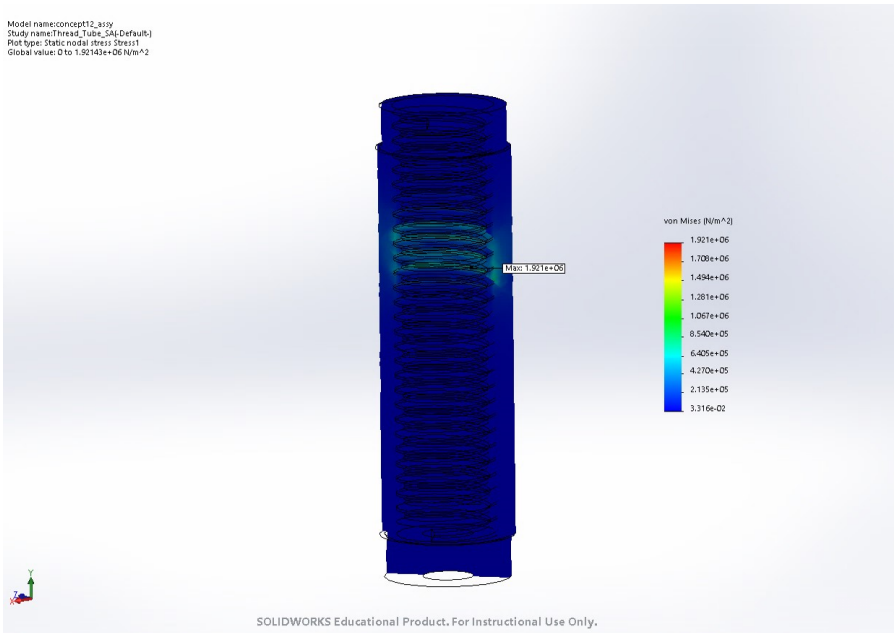

Figure 25: Threaded tube FEA, with a maximum Von Mises stress of 1.9 MPa

E Measurement Data

Multiple tests were performed. Two speed ratio measurments were done. The data is displayed below. There were six load tests performed, while drilling in spruce wood. Their data can be also be found in this appendix.

Speed Ratio Measurement

```
%% Test 1


F0 = 11.0
F1 = 15.2

D0 = 6
D1 = 9
t =0.75

L = 1492

omega = L/(pi*(D0+t))

fr = ((F1-F0)/omega)*1500/60

L_eff =(2*pi*fr)/omega_drill

%% Test 2


F0 =11.1
F1 = 18.15

D0 = 6
D1 = 10.2
t =0.75

L = 2185
omega = L/(pi*(6))

fr = ((F1-F0)/omega)*1500/60

L_eff =(2*pi*fr)/omega_drill
```

Load Measurement

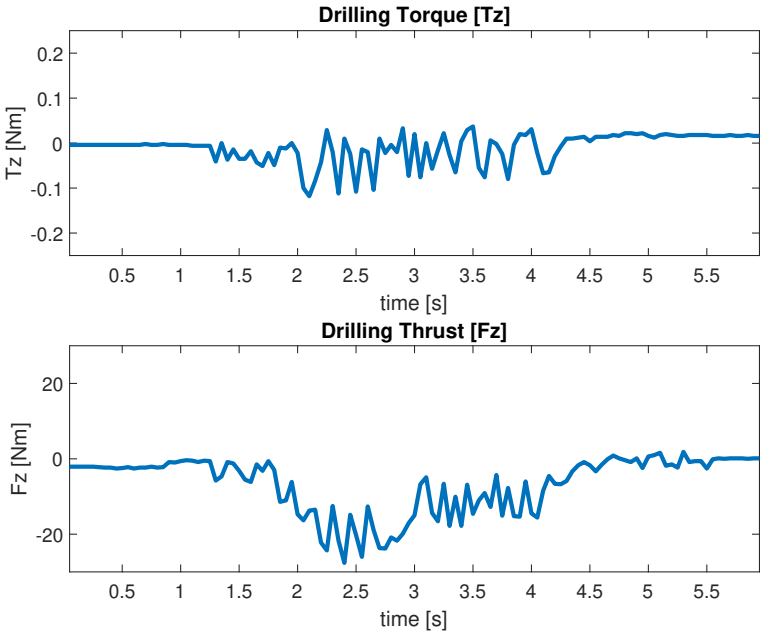

Figure 26: Load measurement 1 data

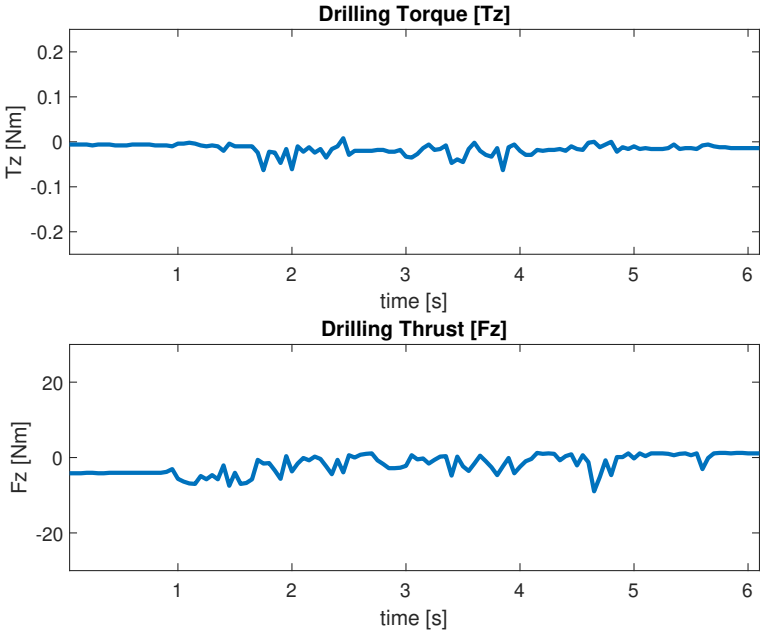

Figure 27: Load measurement 2 data

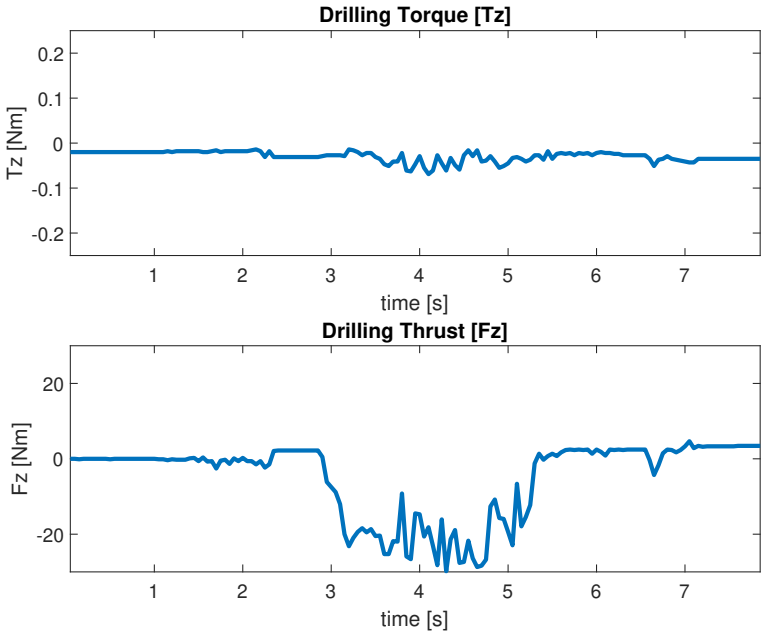

Figure 28: Load measurement 3 data

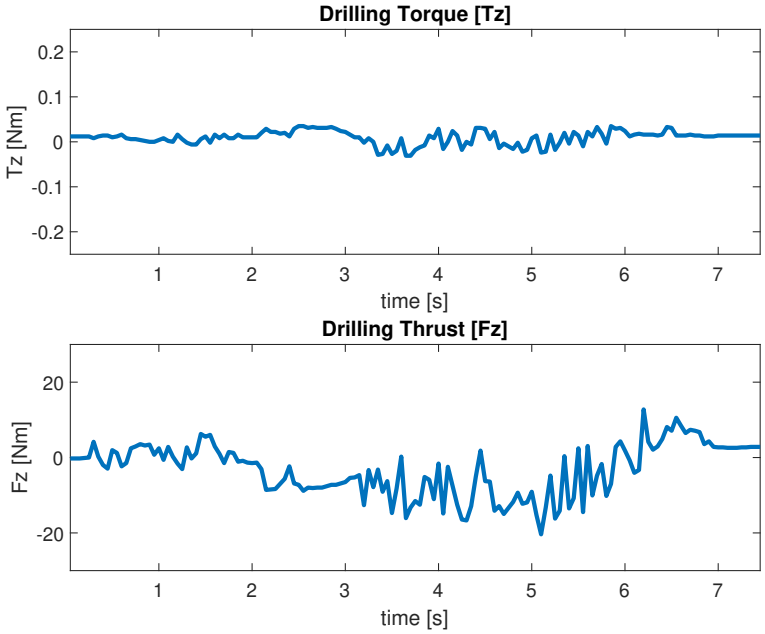

Figure 29: Load measurement 4 data

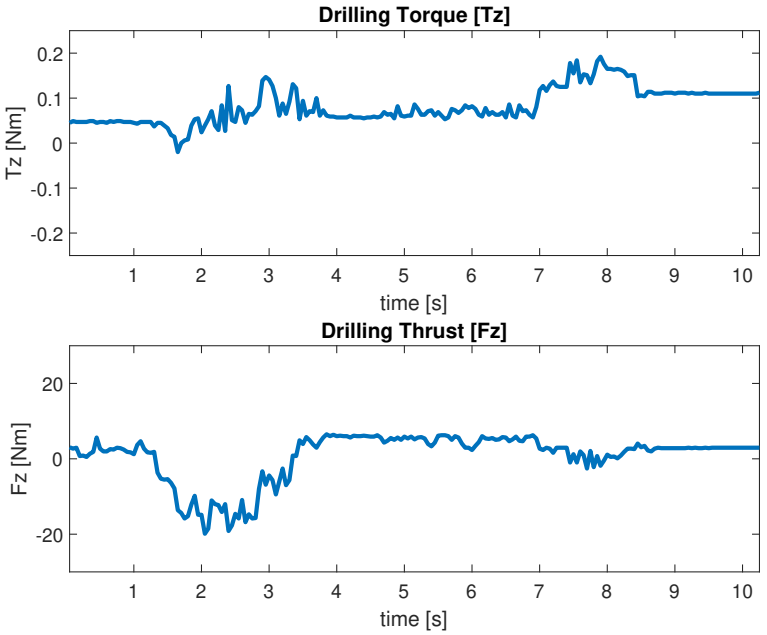

Figure 30: Load measurement 5 data

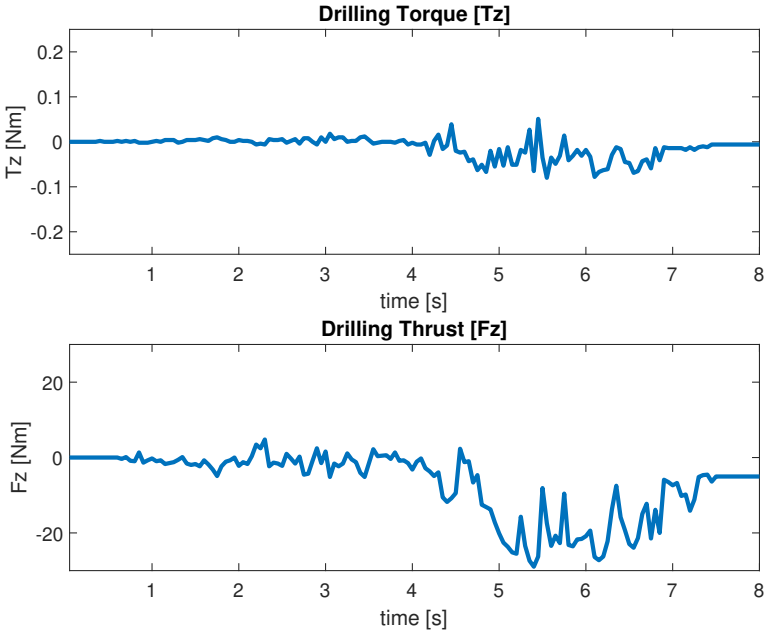

Figure 31: Load measurement 6 data

List of Symbols

η	System efficiency
η_{rot}	Rotational efficiency
η_{thread}	Thread efficiency
η_{trans}	Translational efficiency
λ	Thread lead angle
ν	Feed rate of the drill bit
ω_{drill}	Rotational speed of the drill bit
ω_{in}	Rotational speed of the input shaft
ω_{lag}	Rotational speed of the lag gear
ω_{lead}	Rotational speed of the lead gear
ϕ	Thread friction angle
d	Input shaft diameter
F_{load}	Load force
f_{rot}	Rotational ideal power fraction
f_{trans}	Translational ideal power fraction
L	Thread lead
l	Wire length
L_{eff}	Effective lead
N_{lag}	Number of teeth of the lag gear
N_{lead}	Number of teeth of the lead gear
N_{lobes}	Number of lobes on the cam
N_{pins}	Number of pins on the outside ring
T_{in}	Input torque
T_{load}	Load torque
x_0	Drill bit protrusion at position 0
x_1	Drill bit protrusion at position 1